This is a preprint of an article published in *Microscopy Research and Technique*, **46**, 104-116 (1999).

Direct Methods in Electron Crystallography
— Image processing and solving incommensurate structures

FAN HAI-FU
Institute of Physics, Chinese Academy of Sciences, Beijing 100080, China

KEY WORDS Direct methods, Image processing, Incommensurate Structures, Dynamical diffraction effect

ABSTRACT Theory and practice of direct methods are given in detail for their application in image processing of high resolution electron microscopy and for solving incommensurate crystal structures. The effect of dynamical electron diffraction is also discussed.

INTRODUCTION

For the structure analysis of crystalline materials, electron crystallographic methods are in some cases superior to X-ray methods. Firstly, many crystalline materials important in science and technology, such as high *Tc* superconductors, are too small in grain size and too imperfect in periodicity for an X-ray single crystal analysis to be carried out, but they are suitable for electron microscopic observation. Secondly the atomic scattering factors for electrons differ greatly from those for X-rays and it is easier for electron diffraction to observe light atoms in the presence of much heavier atoms. Finally the electron microscope is the only instrument that can produce simultaneously for a crystalline sample a microscope image and a diffraction pattern at atomic resolution. In principle either the electron microscope image (EM) or the electron diffraction (ED) pattern could lead to a structure image of the sample. However the combination of the two will make the procedure much more efficient and powerful. Solving crystal structures from electron diffraction data based on the kinematical-diffraction approximation were pioneered by Vainshtein and his colleagues (see Vaishtein, 1964) and by Cowley (1953). The first application of direct methods in electron diffraction analysis was presented by Dorset and Hauptman (1976). High resolution electron microscopic observation of crystal structures appeared in early 1970's for inorganic compounds (Allpress, Hewat, Moodie and Sanders, 1972; Cowley and Iijima, 1972) and for the organic compound, chlorinated copper phthalocyanine (Uyeda Kobayashi, Suito, Harada and Watanabe, 1972). The idea of combining the information from an EM and the corresponding ED pattern was proposed by Gerchberg and Saxton (1971). The first attempt to enhance the resolution of an EM by making use of the corresponding ED was reported by Ishizuka, Miyazaki, and Uyeda (1982) using the phase correction method (summarized by Gassmann, 1976). Direct methods in X-ray crystallography were introduced into high resolution electron microscopy as a tool of image processing combining the information from an EM and the corresponding ED (Li and Fan, 1979; Fan and Li, 1987). The procedure is in two stages, i.e. image deconvolution and phase extension. The former aims at eliminating the blurring effect of the contrast transfer function, while the later is for enhancing the resolution of the image. Multidimensional direct methods (Hao, Liu and Fan, 1987; Fan, Van Smaalen, Lam and Beurskens, 1993) have been developed for solving crystal structures containing periodic defects. They have been used to reveal the incommensurate structure modulation in high *Tc* superconductors using electron crystallographic data. The scope of this paper will be concentrated in the direct methods which are applied in electron crystallography for the image processing and for solving incommensurate crystal structures. While the kinematical electron diffraction are assumed for all examples in this paper, the effect of dynamical electron diffraction on the results will be discussed.

IMAGE PROCESSING COMBINING EM AND ED

Simulating calculations with the sample, chlorinated copper phthalocyanine, have shown that the combination of EM and ED can be a much more powerful tool than either of them alone (Fan, Zhong, Zheng and Li, 1985; Han, Fan and Li, 1986). The results are summarized in Figure 1. The object, chlorinated copper phthalocyanine ($C_{32}N_8Cl_{16}Cu$) crystallizes in the space group C2/c with unit cell parameters a=19.62, b=26.08, c=3.76Å and β=116.5^o. Figure 1*a* is the expected image of the unit cell at 1Å resolution projected down the $\boldsymbol{c}$ axis. Figure 1*b* is the theoretical EM at 2Å resolution taken

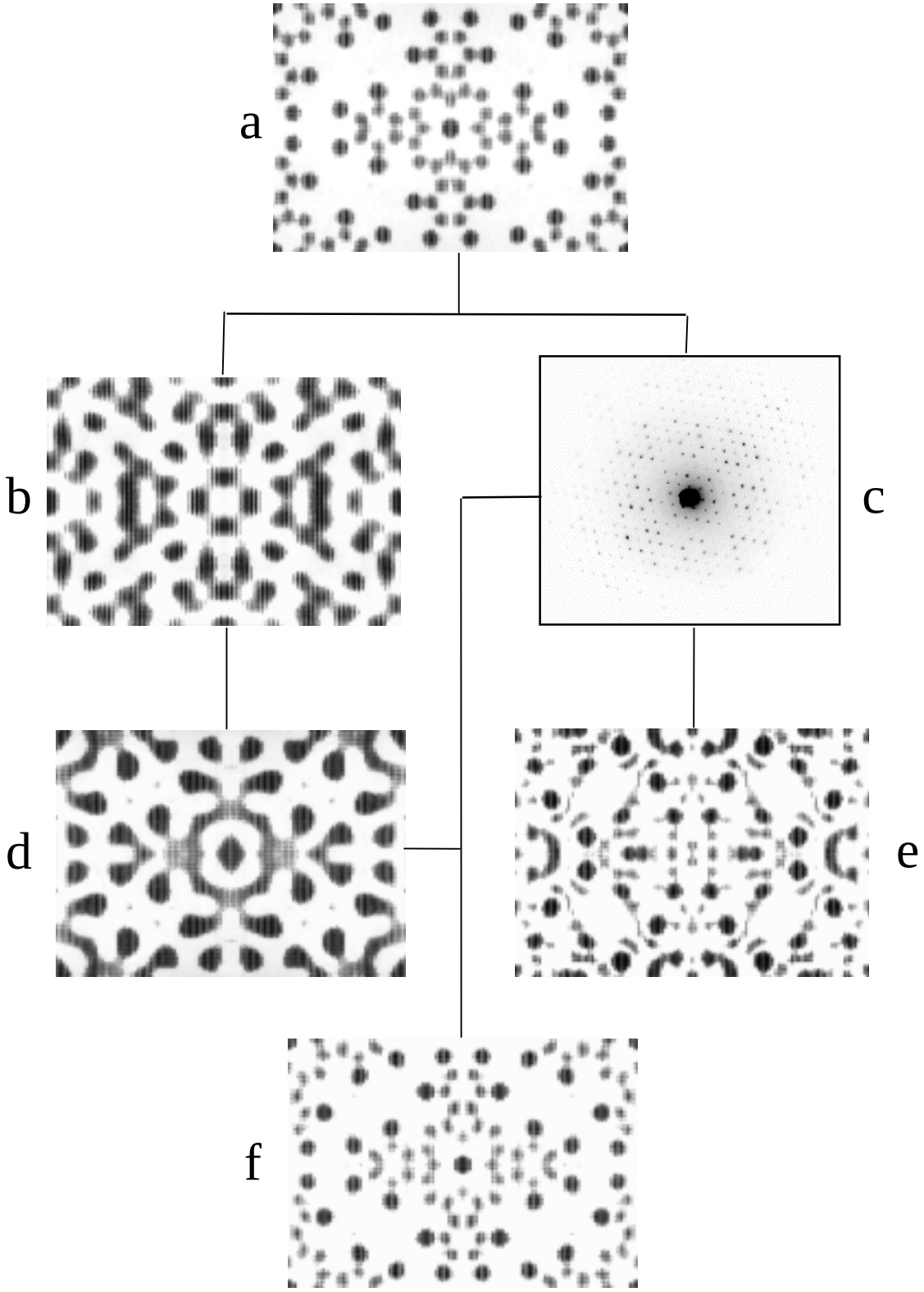

Figure 1. Simulating calculations on the crystalline chlorinated copper phthalocyanine. (a) the expected structure image; (b) the theoretical EM at 2Å resolution; (c) the corresponding ED pattern; (d) the direct-method deconvolution result of (b); (e) the result of direct-method phasing with theoretical electron diffraction data at 1Å resolution; (f) the result of image processing combining EM and ED.

with the photographic conditions: accelerating voltage=500kV, *Cs*=1mm, *D*=150Å and $\Delta f = -1000$Å. Figure 1*c* is the corresponding ED pattern at 1Å resolution. It is seen from Figure 1*b* that, even in the case of kinematical diffraction, an EM will not necessary directly reflect structure details of the object. However a direct-method image deconvolution (Han, Fan and Li, 1986) could bring Figure 1*b* to 1*d*. Here the shape of the molecule can be recognized but individual atoms other than copper are not

visible. On the other hand, a set of structure-factor magnitudes at 1Å resolution can be measured from the ED pattern. *Ab initio* direct-method phasing of these data resulted in the best E-map shown in Figure 1*e*. Although the chlorine atoms are on the map, but the large number of ghost peaks makes the E-map impossible to interpret. With the same set of structure-factor magnitudes, by incorporating the phase information at 2Å resolution obtained from the Fourier transform of Figure 1*d*, a direct-method phase extension (Fan, Zhong, Zheng and Li, 1985) led to Figure 1*f*, which is nearly the same as Figure 1*a*, the theoretical structure image. While the advantage of combining EM and ED is evident, it does not mean that, to solve the structure from an ED alone is impossible. Dorset, Tivol and Turner (1991) and Tivol, Dorset, McCourt and Turner (1993) reported the determination of the structure of chlorinated copper phthalocyanine. They started from an experimental ED pattern at 0.91Å resolution obtained with the accelerating voltage of 1200 kV. Direct-methods phasing of the ED revealed all the heavy atoms. The Fourier refinement based on which let to the complete structure.

Image Deconvolution

The goal of image deconvolution is to retrieve the structure image from one or a series of blurred EMs, or equivalently, to extract a set of structure factors from them. Different procedures have been proposed. Most of them use a series of EMs with different defocus values. Uyeda and Ishizuka (1974, 1975) first proposed a method for the deconvolution of a single EM under the weak-phase-object approximation. Inspired by this work, direct methods in X-ray crystallography were introduced into high resolution electron microscopy for the image deconvolution using a single EM (Li and Fan, 1979; Han, Fan and Li, 1986; Liu, Xiang, Fan, Tang, Li, Pan, Uyeda and Fujiyoshi, 1990).

With the weak-phase-object approximation, in which dynamical diffraction effects are neglected, the Fourier transform of an EM can be expressed as

$$T(\mathbf{h}) = \delta(h) + 2\sigma F(\mathbf{h}) \sin \chi_1(h) \exp[-\chi_2(h)], \tag{1}$$

which can be rearranged to give

$$F(\mathbf{h}) \underset{h\neq 0}{=} T(\mathbf{h})/2\sigma \sin \chi_1(h) \exp[-\chi_2(h)], \tag{2}$$

Here $\sigma = \pi/\lambda U$, λ is the electron wavelength and U the accelerating voltage. **h** is the reciprocal lattice vector within the resolution limit. $F(\mathbf{h})$ is the structure factor of electron diffraction, which is the Fourier transform of the potential distribution $\varphi(\mathbf{r})$ of the object. $\sin\chi_1(h)\exp[-\chi_2(\boldsymbol{h})]$ is the contrast transfer function, in which

$$\chi_1(h) = \pi\Delta f\lambda h^2 + \frac{1}{2}(\pi C_s \lambda^3 h^4),$$

$$\chi_2(h) = \frac{1}{2}(\pi^2 \lambda^2 h^4 D^2).$$

Here Δf is the defocus value, C_s is the spherical aberration coefficient and D is the standard deviation of the Gaussian distribution of defocus due to the chromatic aberration (Fijes,1977). The values of Δf, C_s and D should be found by image deconvolution. Of these three factors, C_s and D can be determined experimentally without much difficulties. Further more, in contrast to Δf, C_s and D do not change much from one image to another. This means that the main problem is the evaluation of Δf. With the estimated values of C_s and D, a set of $F(\mathbf{h})$ can be calculated from Equation (2) for a given value of Δf. If the Δf value is correct then the corresponding set of $F(\mathbf{h})$ should obey the Sayre equation (Sayre, 1952)

$$F_{\mathbf{h}} = \frac{\theta}{V} \sum_{\mathbf{h}'} F_{\mathbf{h}'} F_{\mathbf{h}-\mathbf{h}'}, \tag{3}$$

where θ is the atomic form factor and V is the volume of the unit cell. Hence the true Δf can be found by a systemic change of the trial Δf so as to improve the validity of the Sayre equation. For the evaluation of the quality of each trial, figures of merit used for direct methods in X-ray crystallography (see

Woolfson and Fan, 1995) were introduced. The procedure has been automated in the program *VEC* (Wan, Fu, and Fan, 1997). An example $K_2O.7Nb_2O_5$ is given here. The space group is P4bm and unit cell parameters are a=b=27.5Å and c=3.94Å. Figure 2*a* is the expected image at 3Å resolution of the unit cell projected down the ***c*** axis. Two [001] direction experimental EMs at the same resolution, one near to and the other far from the optimum defocus, are shown in Figures 2*b* and

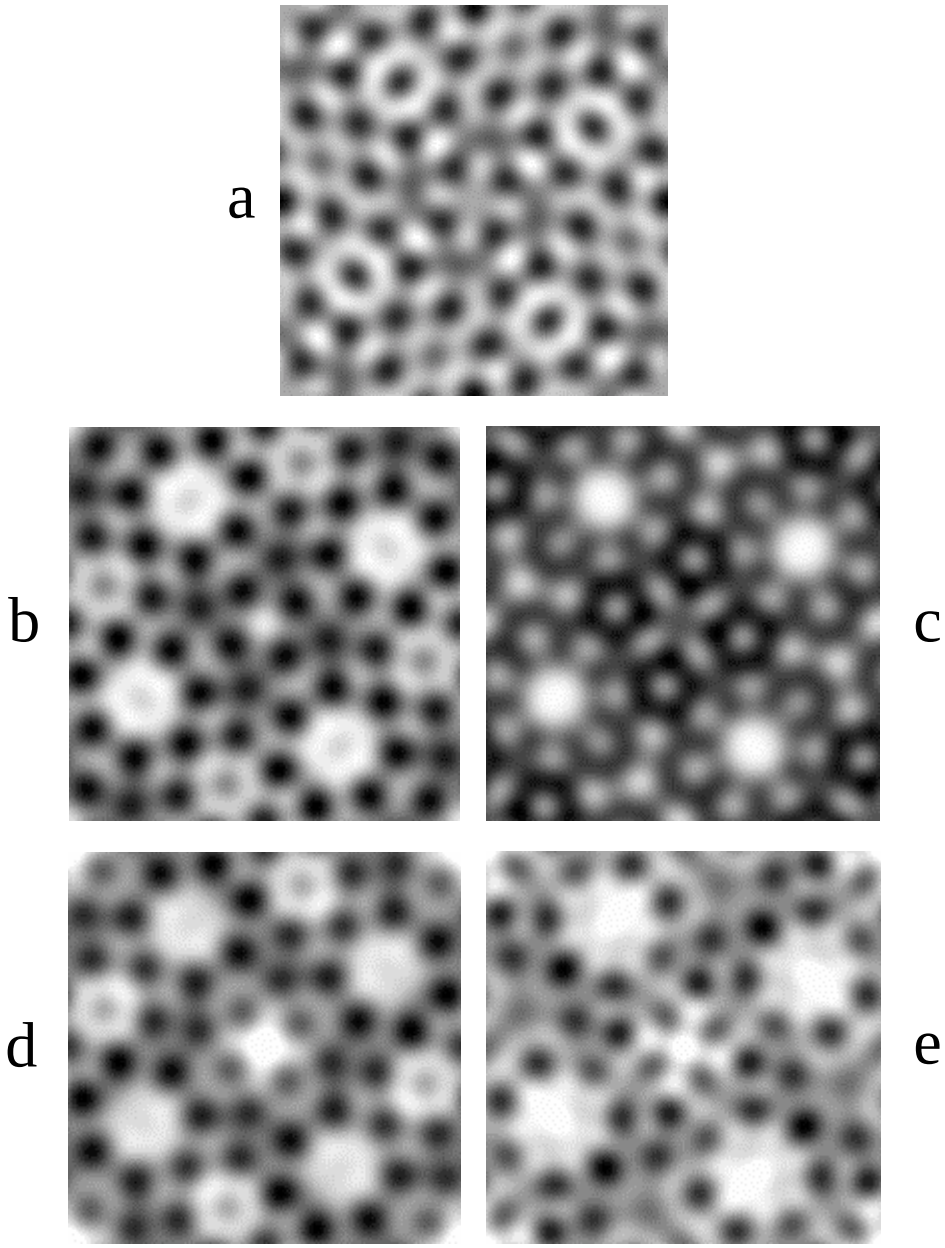

Figure 2. Image deconvolution of high resolution EMs of $K_2O.7Nb_2O_5$. (a) the expected structure image at 3Å resolution; (b) and (c): experimental EMs with defocus value at about −900Å and −400Å respectively; (d) and (e): deconvoluted images of (b) and (c) respectively.

2*c* respectively. It is seen that Figure 2*b* and 2*c* are quite different and roughly the inverse to each other. Starting with the images 2*b* and 2*c* respectively, the program *VEC* (Wan, Fu and Fan, 1997) resulted in the deconvoluted images 2*d* and 2*e*. Now both the two deconvoluted images have the similar feature as that of the expected image 2*a*, *i.e*. they all have four heptagonal channels surrounding by hexagonal, pentagonal, tetragonal and trigonal channels.

As has been shown by the simulating calculation (Han, Fan and Li, 1986), ED data can help improving the deconvolution result. An example using real experimental data is given on the left part of Figure 3. By comparing Figure 3*a*, 3*b* and 3*d*, it is seen that even for an EM taken under the optimum defocus condition, the image quality can be significantly improved by the deconvolution making use of the corresponding ED data.

Phase Extension

An ED pattern usually contains observable reflections at the resolution equal to or better than 1Å. In addition, the intensities of the ED pattern from a crystalline specimen are independent of defocus and the spherical aberration of the electron-optical system. Accordingly, under the weak-phase-object approximation, better quality images could be obtained from ED. However, structure analysis by ED alone is subject to the well-known difficulty of the crystallographic phase problem (but see Dorset, Tivol and Turner, 1991; 1992). On the other hand, since an EM, after deconvolution, can provide phase information at about 2Å resolution, the complexity of the solution of the phase problem can be greatly reduced. An improved high-resolution image can be obtained by a phase extension procedure using the magnitudes of the structure factors from ED and starting phases from the corresponding EM. The tangent formula (Karle and Hauptman, 1956) is used as the basis of the phase extension:

$$\tan a_{\mathbf{h}} = \frac{\sum_{\mathbf{h}'} \left| E_{\mathbf{h}'} E_{\mathbf{h}-\mathbf{h}'} \right| \sin(a_{\mathbf{h}'} + a_{\mathbf{h}-\mathbf{h}'})}{\sum_{\mathbf{h}'} \left| E_{\mathbf{h}'} E_{\mathbf{h}-\mathbf{h}'} \right| \cos(a_{\mathbf{h}'} + a_{\mathbf{h}-\mathbf{h}'})}, \qquad (4)$$

where $\alpha_{\mathbf{h}}$ is the phase associated with the normalized structure factor $E_{\mathbf{h}}$. The later is in turn expressed by the conventional structure factor F_{h} as

$$E_{\mathbf{h}} = F_{\mathbf{h}} \quad / (\varepsilon \sum \quad)^{1/2}.$$

Σ is the average value of $|F_{\mathbf{h}}|^2$ for the scattering angle corresponding to **h**. The factor ε usually equals unity but is, in general, a small integer that depends on the space group and the type of reflection and gives the effect that for all the reflections of that particular type $\langle |E_{\mathbf{h}}|^2 \rangle = 1$.

By substituting the normalized structure factors with known phases into the right-hand side of the tangent formula, originally unknown phases can be predicted according to the outcome on the left-hand side. In the program *VEC* a procedure similar to that of *RANTAN* (Yao, 1981) is used for phase extension. All reflections with their *E* value greater than a certain limit are put into the right-hand side of Equation (4). Trial sets of random values are given to the unknown phases. The random phases in each trial set are then changed gradually during the recycling process until they are converged. Figures of merit (see Woolfson and Fan, 1995) are used to pick out the best solution from the resulting phase sets.

An example of phase extension using the experimental EM and ED of chlorinated copper phthalocyanine is given below. Structure-factor magnitudes up to 1Å resolution were measured from the ED pattern, Figure 3*c*. Phases up to 2Å resolution were obtained from the Fourier transform of the deconvoluted image, Figure 3*d*. The phase extension with the program *VEC* resulted in Figure 3*e*, which shows the essential features of the structure at atomic resolution. Four cycles of Fourier iteration based on this gave significant improvement as is shown in Figure 3*f*. This work was originally done by Fan, Xiang, Li, Pan, Uyeda and Fujiyoshi (1991). The results shown here were reproduced with improvements by using the program *VEC* (Wan, Fu and Fan, 1997).

Fan and Zheng (1975) have shown that it is possible to extrapolate not only the phases but also the magnitudes of structure factors beyond the resolution limit of the original diffraction data. An example of the structure-factor extrapolation from the theoretical EM of chlorinated copper phthalocyanine at 2Å resolution to the structure image at 1Å resolution has been reported by Liu, Fan and Zheng (1988). Applications to real EMs still have to be explored.

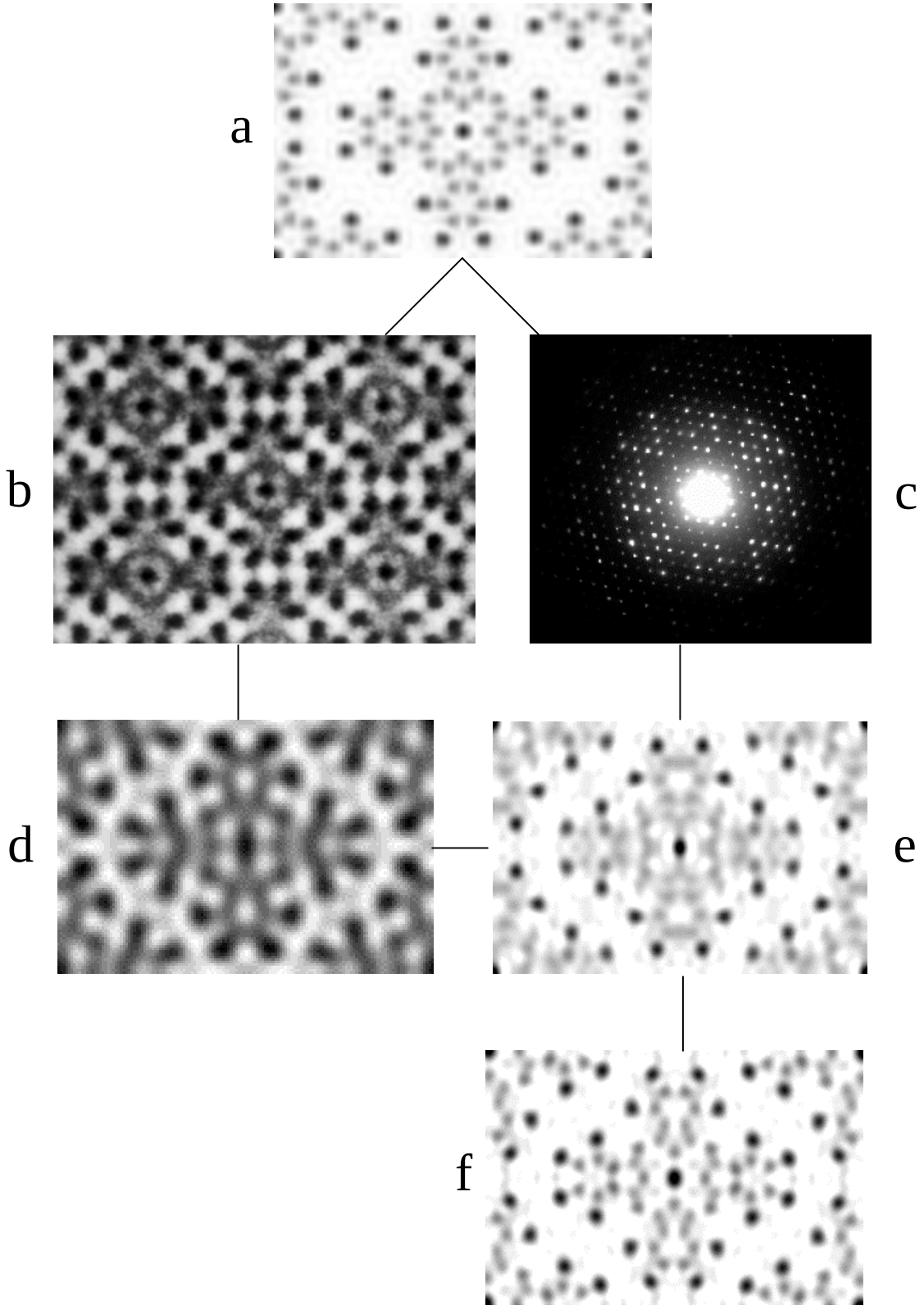

Figure 3. Image processing of the high resolution EM of chlorinated copper phthalocyanine. (a) the expected structure image of the object projected along the ***c*** axis; (b) the experimental EM of the object at 2Å resolution taken near the optimum defocus value; (c) the corresponding experimental ED pattern; (d) the direct-method deconvoluted image of (b); (e) the electron potential projection of the object at 1Å resolution obtained from the direct-method phase extension based on the deconvoluted image at 2Å resolution and experimental electron diffraction data at 1Å resolution. (f) the electron potential projection after 4 cycles of Fourier refinement. The experimental EM and ED are provided by Professor N. Uyeda.

MULTIDIMENSIONAL DIRECT METHODS AND THE DETERMINATION OF INCOMMENSURATE CRYSTAL STRUCTURES

In diffraction analysis, crystal structures are assumed to be ideal 3-dimensional periodic objects. Since real crystals are never perfect, what we obtained is just an averaged image of the real structure over a large number of unit cells. However a knowledge on the average structure is not enough for understanding the properties of many solid state materials. Therefore an important task for methods of solving crystal structures is to extend their scope to include real crystals. Modulated crystal structures belong to that kind of crystal structures, in which atoms suffer from certain occupational and/or positional fluctuation. If the period of fluctuation is commensurate with that of the three-dimensional unit cell then a superstructure results, otherwise an incommensurate modulated structure is obtained. Incommensurate modulated phases can be found in many important solid state materials. In many cases, the transition to the incommensurate modulated structure corresponds to a change of certain physical properties. Hence it is important to know the structure of incommensurate modulated phases in order to understand the mechanism of the transition and properties in the modulated state. Up to the present many incommensurate modulated structures were solved by trial-and-error methods. With these methods it is necessary to make assumption on the modulation in advance. This leads often to difficulties or erroneous results. In view of diffraction analysis, it is possible to phase the reflections directly and solve the structure objectively without relying on any assumption about the modulation wave. Multidimensional direct methods have been developed for this purpose (Hao, Liu and Fan, 1987; Fan, Van Smaalen, Lam and Beurskens, 1993). A brief description of the theory involved is given below.

An incommensurate modulated structure produces a 3-dimensional diffraction pattern, which contains satellites round the main reflections. An example of a section of such a 3-dimensional diffraction pattern is shown schematically in Figure 4.

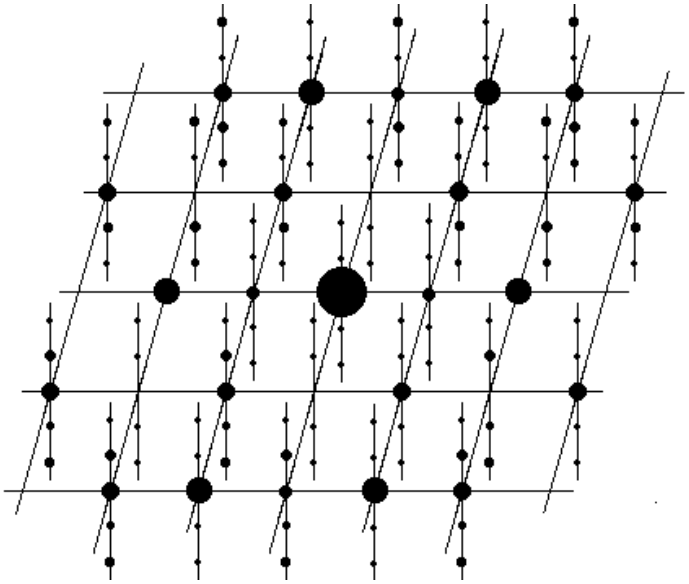

Figure 4. Schematic diffraction pattern of an incommensurate modulated structure. The vertical line segments indicate projected lattice lines parallel to the fourth dimension

The main reflections are consistent with a regular 3-dimensional reciprocal lattice but the satellites do not fit the same lattice. On the other hand, while the satellites are not commensurate with the main reflections, they have their own periodicity. Hence, it can be imagined that the 3-dimensional diffraction pattern is a projection of a 4-dimensional reciprocal lattice, in which the main and the satellite reflections are all regularly situated at the lattice nodes. From the properties of the Fourier transform the incommensurate modulated structure here considered can be regarded as a 3-dimensional "section" of a 4-dimensional periodic structure. This representation was first proposed by De Wolff (1974) to simplify the structure analysis of the incommensurate modulated structure of γ-Na_2CO_3. The above example corresponds to a one-dimensional modulation. For an n-dimensional (n=1,2, …) modulation, it needs a (3+n)-dimensional description. A (3+n)-dimensional reciprocal vector is

expressed as

$$\mathbf{h} = h_1\mathbf{b}_1 + h_2\mathbf{b}_2 + h_3\mathbf{b}_3 + \ldots + h_{3+n}\mathbf{b}_{3+n} \qquad (n = 1,2,\ldots) \tag{5}$$

where $\mathbf{b}_i$ is the i^{th} translation vector defining the reciprocal unit cell. The structure factor formula is written as

$$F(\mathbf{h}) = \sum_{j=1}^{N} f_{j(\text{mod})}(\mathbf{h}) \exp[i2\pi(h_1\bar{x}_{j1} + h_2\bar{x}_{j2} + h_3\bar{x}_{j3})] \tag{6}$$

where

$$\begin{aligned} f_{j(\text{mod})}(\mathbf{h}) = {} & f_j(h)\int_0^1 d\,\bar{x}_4 \ldots \int_0^1 d\,\bar{x}_{3+n} P_j(\bar{x}_4,\ldots,\bar{x}_{3+n})\times \\ & \exp\{i2\pi[(h_1U_{j1} + h_2U_{j2} + h_3U_{j3}) + (h_4x_{j4} + \ldots + h_{3+n}x_{j(3+n)})]\} \end{aligned} \tag{7}$$

The $f_j(h)$ on the right-hand side of (7) is the ordinary atomic scattering factor, P_j is the occupational modulation function and U_j describes the deviation of the j^{th} atom from its average position $(\bar{x}_{j1}, \bar{x}_{j2}, \bar{x}_{j3})$. For more details on (6) and (7) the reader is referred to the papers by De Wolff (1974), Yamamoto (1982) and Hao, Liu & Fan (1987). What should be emphasised here is that, according to (6) a modulated structure can be regarded as a set of 'modulated atoms' situated at their average positions in 3-dimensional space. The 'modulated atom' in turn is defined by a 'modulated atomic scattering factor' expressed as (7). A special kind of incommensurate modulated structures is called composite structures. The characteristic of which is the coexistence of two or more mutually incommensurate 3-dimensional lattices. Owing to the interaction of coexisting lattices, composite structures are also incommensurate modulated structures. Unlike ordinary incommensurate modulated structures, composite structures do not have a 3-dimensional average (basic) structure. The basic structure of a composite structure corresponds to a 4- or higher-dimensional periodic structure. For a detailed description of composite structures the reader is referred to the paper by Van Smaalen (1992). Obviously crystal-structure analysis of incommensurate modulated structures would better be implemented in multi-dimensional space. For this purpose we need firstly a theory on multi-dimensional symmetry and secondly a method to solve directly the multi-dimensional phase problem. The work of Janner and co-workers (see Janssen, Janner, Looijenga-Vos and De Wolff, 1992) has been aiming at the first problem, while the multidimensional direct methods are trying to solve the second.

Hao, Liu and Fan (1987) showed that the Sayre equation (1952) can be extended into multi-dimensional space. We have

$$F(\mathbf{h}) = \frac{\theta}{V}\sum_{\mathbf{h}'} F(\mathbf{h}')F(\mathbf{h}-\mathbf{h}'), \tag{8}$$

here **h** is a multi-dimensional reciprocal vector defined as (5). The right-hand side of (8) can be split into three parts, i.e.

$$F(\mathbf{h}) = \frac{\theta}{V}\left\{\sum_{\mathbf{h}'} F_{\text{m}}(\mathbf{h}')F_{\text{m}}(\mathbf{h}-\mathbf{h}') + 2\sum_{\mathbf{h}'} F_{\text{m}}(\mathbf{h}')F_{\text{s}}(\mathbf{h}-\mathbf{h}') + \sum_{\mathbf{h}'} F_{\text{s}}(\mathbf{h}')F_{\text{s}}(\mathbf{h}-\mathbf{h}')\right\}. \tag{9}$$

Where subscript *m* stands for main reflections while subscript *s* stands for satellites. Since the intensities of satellites are on average much weaker than those of main reflections, the last summation on the right-hand side of (9) is negligible in comparison with the second, while the last two summations on the right-hand side of (9) are negligible in comparison with the first. Letting $F(\mathbf{h})$ on the left-hand side of (9) represents only the structure factor of main reflections we have to first approximation

$$F_{\text{m}}(\mathbf{h}) \approx \frac{\theta}{V}\sum_{\mathbf{h}'} F_{\text{m}}(\mathbf{h}')F_{\text{m}}(\mathbf{h}-\mathbf{h}'). \tag{10}$$

On the other hand, if $F(\mathbf{h})$ on the left-hand side of (9) corresponds only to satellites, it follows that

$$F_s(\mathbf{h}) \approx \frac{\theta}{V}\sum_{\mathbf{h'}} F_m(\mathbf{h'})F_m(\mathbf{h}-\mathbf{h'}) + \frac{2\theta}{V}\sum_{\mathbf{h'}} F_m(\mathbf{h'})F_s(\mathbf{h}-\mathbf{h'}) . \qquad (11)$$

For ordinary incommensurate modulated structures the first summation on the right-hand side of (11) has vanished, because any three-dimensional reciprocal lattice vector corresponding to a main reflection will have zero components in the extra dimensions so that the sum of two such lattice vectors could never give rise to a lattice vector corresponding to a satellite. We then have

$$F_s(\mathbf{h}) \approx \frac{2\theta}{V}\sum_{\mathbf{h'}} F_m(\mathbf{h'})F_s(\mathbf{h}-\mathbf{h'}) . \qquad (12)$$

For composite structures on the other hand, since the average structure itself is a 4- or higher-dimensional periodic structure, the first summation on the right-hand side of (11) does not vanish. We have instead of (12) the following equation:

$$F_s(\mathbf{h}) \approx \frac{\theta}{V}\sum_{\mathbf{h'}} F_m(\mathbf{h'})F_m(\mathbf{h}-\mathbf{h'}) . \qquad (13)$$

Equation (10) indicates that the phases of main reflections can be derived by a conventional direct method neglecting the satellites. Equation (12) or (13) can be used to extend phases from the main reflections to the satellites respectively for ordinary incommensurate modulated structures or composite structures. This provides a way to determine the modulation functions objectively. The procedure will be in the following stages:

i) derive the phases of main reflections using Equation (10);
ii) derive the phases of satellite reflections using Equation (12) or (13);
iii) calculate a multi-dimensional Fourier map using the observed structure factor magnitudes and the phases from i) and ii);
iv) cut the resulting Fourier map with a 3-dimensional 'hyperplane' to obtain an 'image' of the incommensurate modulated structure in the 3-dimensional physical space;
v) parameters of the modulation functions are measured directly on the multi-dimensional Fourier map resulting from iii).

A program package *DIMS* (Direct methods for Incommensurate Modulated Structures) has been written in Fortran for the implementation of steps i) and ii) (Fu and Fan, 1994; Fu and Fan, 1997).

The widespread occurrence of incommensurate modulations in the high-*Tc* superconducting phases and related compounds requires the multi-dimensional crystallographic methods for their structure analysis. On the other hand, the modulation in the high-*Tc* superconductors involves both the metal and the oxygen atoms. The modulation of the latter in the Bi-O layer is important for understanding the mechanism of superconductivity, since it plays an important role in the incorporation of extra O atoms in the Bi-O layer and hence contributes to the hole concentration in the Cu-O layer. Owing to the dominating effect of heavy atoms in X-ray diffraction, electron diffraction can be a better technique to study the oxygen modulation. In the following there are examples on studying structure details of high-*Tc* superconductors by multidimensional direct methods with electron crystallographic data.

The Incommensurate Modulation of the Pb-Doped Bi-2223 Superconductor

The analysis was based on the preliminary electron diffraction study of Li *et al.* (1989) and the average structure obtained by Sequeira *et al.* (1990). The diffraction intensities used in the study were

measured from the electron diffraction pattern normal to the ***a*** axis. Since the ***a*** axis is rather short (5.49Å) and is perpendicular to the modulation vector ***q***, no attempt was made to use 3-dimensional diffraction data. The symmetry of the sample belongs to the superspace group P [B bmb] 1-11 (see Janssen et al., 1992, for a discussion of superspace groups and their designations.) with the 3-dimensional unit cell $a = 5.49$, $b = 5.41$, $c = 37.1$Å; $\alpha = \beta = \gamma = 90^{o}$ and the modulation vector $\boldsymbol{q} = 0.117\boldsymbol{b}^*$. Five photographs were taken with different exposure times for the same *0klm* electron diffraction pattern. This is an analogue of the multifilm method in X-ray crystallography for collecting diffraction intensities. A microdensitometer was used to measure the integrated intensities. Structure factor magnitudes were obtained as the square root of diffraction intensities. The *R* factor for the discrepancy of symmetrically related reflections is 0.12 for the 42 main reflections and 0.13 for the 70 first-order satellite reflections. A few second-order satellites were also observed; however, they are much weaker than the first-order ones and were neglected in the structure analysis. The structure analysis was carried out in 4-dimensional space, in which the real and the reciprocal unit cells are defined respectively as

$$\boldsymbol{a}_1 = \boldsymbol{a}, \quad \boldsymbol{a}_2 = \boldsymbol{b} - 0.117\boldsymbol{d}, \quad \boldsymbol{a}_3 = \boldsymbol{c}, \quad \boldsymbol{a}_4 = \boldsymbol{d}$$

and

$$\boldsymbol{b}_1 = \boldsymbol{a}^*, \quad \boldsymbol{b}_2 = \boldsymbol{b}^*, \quad \boldsymbol{b}_3 = \boldsymbol{c}^*, \quad \boldsymbol{b}_4 = 0.117\,\boldsymbol{b}^* + \boldsymbol{d}$$

where ***d*** is the unit vector normal to the 3-dimensional space, i.e. a unit vector simultaneously perpendicular to the vectors ***a***, ***b***, ***c***, ***a****, ***b**** and ***c****. An atom in the 4-dimensional space without modulation will be something like an infinite straight bar parallel to the fourth dimension $\boldsymbol{a}_4$. Occupational modulation will change periodically the width, while positional modulation will change periodically the direction of the bar. Our task is to find out such a periodic change. This can be accomplished by solving the phase problem and calculating the 4-dimensional potential distribution, the 4-dimensional Fourier map. The incommensurate modulated structure in the 3-dimensional physical space can be obtained by cutting the 4-dimensional Fourier map with a 3-dimensional hyperplane perpendicular to the direction $\boldsymbol{a}_4$. The modulation wave of all the atoms can be measured directly on the 4-dimensional Fourier map.

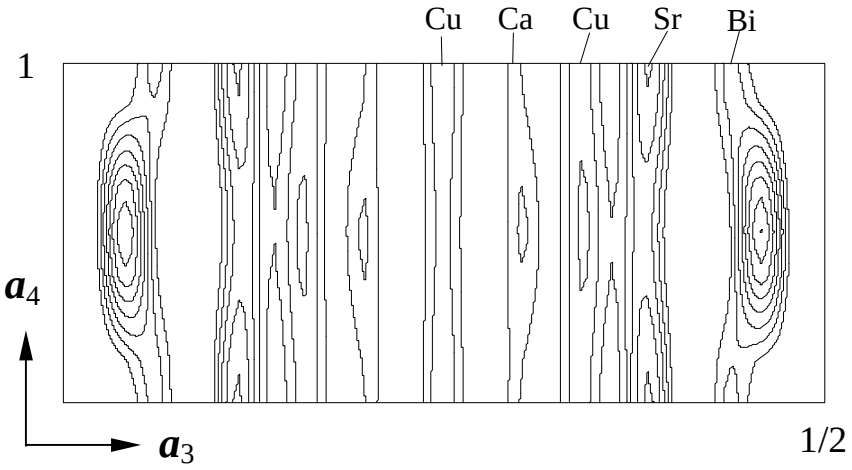

Figure 5. Modulation waves in the Pb-doped Bi-2223 superconductor, revealed on the map $\int \varphi(x_1,0,x_3,x_4)dx_1$, a 3-dimensional 'section' of the 4-dimensional Fourier map at $x_2=0$ projected along the ***a*** axis.

The phases of the main reflections *0kl0* were calculated from the known average structure, while phases of the satellites *0klm* were derived by the multidimensional direct method. A Fourier map in multidimensional space was then calculated, from which modulation waves of all metal atoms were measured directly. On this basis least-square refinement including also modulation parameters of oxygen atoms ended at an *R*-factor of 0.16 for the main and 0.17 for the first-order satellite reflections. *Figure* 5 shows the modulation waves of the metal atoms. *Figure* 6 shows the incommensurate modulation of the Pb-doped Bi-2223 superconductor in the 3-dimensional physical

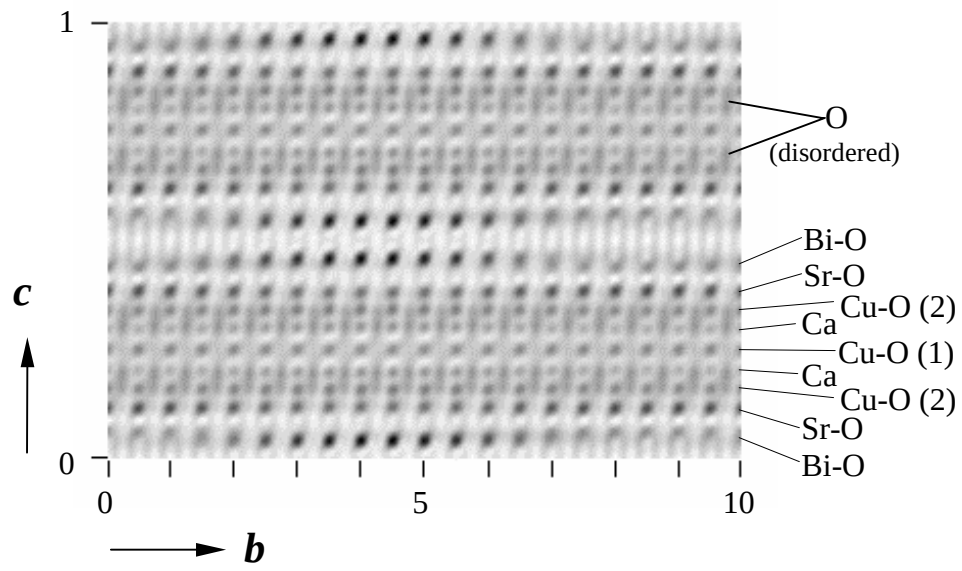

Figure 6. The 3-dimensional potential distribution function of the Pb-doped Bi-2223 superconductor projected along the ***a*** axis on an area of 10*b*×1*c*.

space projected along the ***a*** axis. As is seen, both occupational and positional modulations are evident for most metal atoms. An other prominent feature is that the oxygen atoms on the Cu-O layers move towards the Ca layer, forming a disordered oxygen bridge across the layers of Cu(2)-Ca-Cu(1)-Ca-Cu(2). This work was originally done by Mo *et al*. (1992). The figures shown here were reproduced by using the program *VEC*.

The Incommensurate Modulation of Bi-2212

The superconducting phase Bi-2212 has been extensively studied (Matsui *et al*., 1988; Gao *et al*., 1988; Petricek *et al*., 1990; Yamamoto *et al*., 1990; Kan, *et al*., 1992; Gao *et al*., 1993; Fu *et al*., 1995). Most of them were done using X-ray and/or neutron diffraction data. We provide here an example of using electron crystallographic data and show how the combination of EM and ED can be used to determine the incommensurate structure even when the average structure is unknown (Fu, Huang *et al*., 1994). The sample belongs to the superspace group N [B bmb] 1-11 with a = 5.42, b = 5.44, c = 30.5Å, $\alpha = \beta = \gamma = 90^{o}$ and the modulation wave vector $\boldsymbol{q} = 0.22\,\boldsymbol{b}^* + \boldsymbol{c}^*$. We started with an EM at 2Å resolution (Figure 7*a*) and the corresponding ED (Figure 7*b*) at 1Å resolution. A set of structure-factor magnitudes with indices *0klm* was measured from the ED. The phases of the main reflections within 2Å resolution were obtained from the Fourier transform of the deconvoluted EM. Phases of the satellite reflections and of the main reflections beyond 2Å resolution were derived by the direct-method phase extension using the program *DIMS* (Fu and Fan, 1994). The resulting Fourier map is shown in Figure 7*c*, which reveals much more structure details in comparison with the original EM.

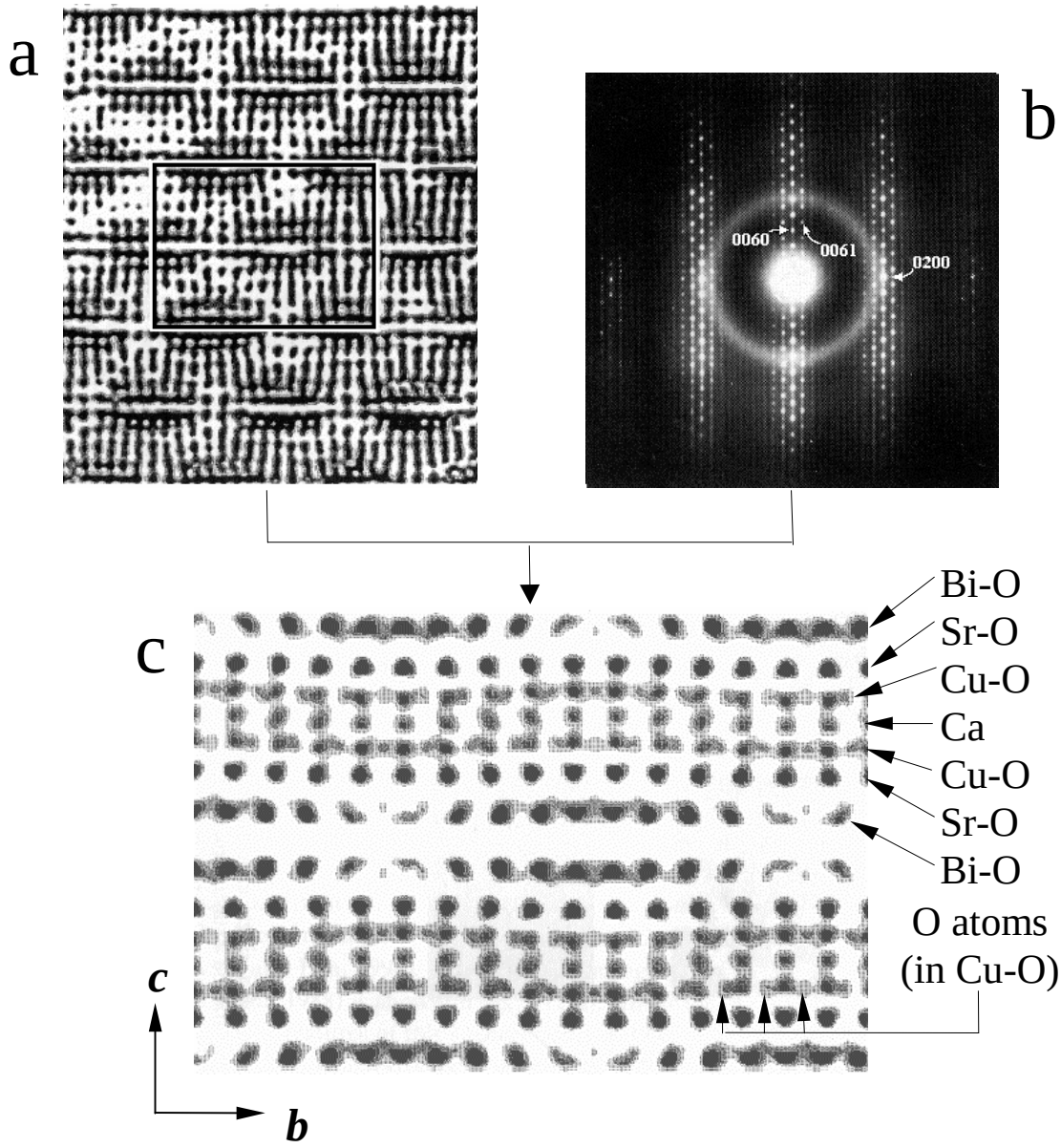

Figure 7. Image processing for the Bi-2212 superconductor. (a) experimental EM taken with the incident electron beam parallel to the ***a*** axis; (b) the corresponding ED pattern; (c) the 3-dimensional potential distribution projected along the ***a*** axis on an area of 8*b*×1*c*. The structure-factor magnitudes used for calculating (c) were from the ED, while the phases were from the direct-method phase extension based on the deconvolution of (a). The experimental EM is provided by Dr. S. Horiuchi.

The Incommensurate Modulation of Bi-2201

Crystals of Bi-2201 belong to the superspace group P [B 2/b] -11 with $a = 5.41$, $b = 5.43$, $c = 24.6$Å, $\alpha = \beta = \gamma = 90^o$ and the modulation wave vector $\boldsymbol{q} = 0.217\boldsymbol{b}^* + 0.62\boldsymbol{c}^*$. The structure analysis was based on the known average structure (Gao, *et al*., 1989). Only electron diffraction intensities of the *0klm* reflections were used. Since inconsistent results have been reported on the oxygen atoms (Gao, *et al*., 1989; Yamamoto *et al*., 1992), special care was taken for their determination. The 4-dimensional Fourier map projected along the ***a*** axis was calculated with phases from the average structure and the direct-method phase extension. Apart from two oxygen atoms, which are overlapped with metal atoms respectively on the Bi-O and Sr-O layers, the modulation waves of all symmetrically independent atoms were measured directly from this Fourier map. Up to the fourth-order harmonics were included in the expression of the modulation function. Fourier recycling and least-squares refinement led to the *R* factors: $R_T = 0.32$, $R_M = 0.29$, $R_{S1} = 0.29$, $R_{S2} = 0.36$ and $R_{S3} = 0.52$. Here the *R* factor is defined as $R = \Sigma| |Fo|-|Fc| |\Big/ \Sigma|Fo|$, R_T denotes the *R* factor for the total reflections, R_M for the main reflections, R_{S1}, R_{S2} and R_{S3} respectively for the first-order, second-order and third-order satellite reflections. The resulting Fourier map clearly shows the main feature of the modulation. However, it contains a number of small additional peaks near some of the Bi and Sr sites.

After failed to eliminate them, they were treated as extra oxygen atoms. By including extra oxygen atoms in the Bi-O layer, a few cycles of refinement brought the *R* factors to 0.23, 0.20, 0.24, 0.27 and 0.30 for R_T, R_M, R_{S1}, R_{S2} and R_{S3} respectively. Further inclusion of extra oxygen atoms in the Sr-O layer led to the *R* factors of 0.18, 0.13, 0.19, 0.25 and 0.26 for R_T, R_M, R_{S1}, R_{S2} and R_{S3} respectively. The final Fourier map is shown in Figure 8.

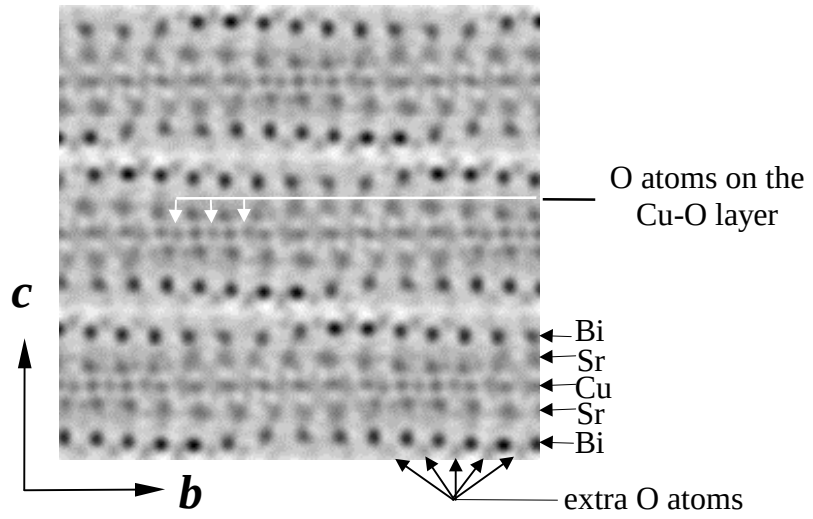

Figure 8. The final Fourier map (three-dimensional potential distribution) of the Bi-2201 superconductor projected down the ***a*** axis on to an area of 7***b***×3***c***.

Solving Composite Structures

There have been no examples on solving composite structures by multidimensional direct methods using electron diffraction data. We provide here an example from X-ray crystallography since the subject is of interesting and the method can be used with electron diffraction data as well. For composite structures it is much more difficult to solve the average structure than to determine the modulation. The reason is that, the average structure of a composite crystal corresponds to a four- or higher-dimensional periodic object and, *ab initio* phasing rather than phase extension should be used for solving the phase problem. However by using multidimensional direct methods the problem can be much simpler. The composite crystal structure $(PbS)_{1.18}TiS_2$ (Van Smaalen et al., 1991) belongs to the space group C2/m (α, *0*, *0*) s-1. It consists of two subsystems: the subsystem TiS_2 with a_1=3.409, *b*=5.880, *c*=11.760 α=95.29° and the subsystem *PbS* with a_2=5.800, *b*=5.881, *c*=11.759 α=95.27°. A default run of *DIMS* in a test (Mo *et al.*, 1996) using Equation (10) was able to reveal directly the basic structure (see Figure 9). On the upper-left of Figure 9 there is the direct-method-resulting electron density map, which is the 3-dimensional hypersection with $x_4 = 0$ projected along the ***b*** axis. The map shows the alternate stacking of TiS_2 and *PbS* layers along the ***c*** axis. This results in a 'chimney-ladder' structure along the ***a*** axis with two incommensurate periodicity a_1 and a_2. The other three direct-method maps in Figure 9 are 2-dimensional sections of the 4-dimensional electron density function showing clearly all the atoms in the unit cell. Determination of the modulation by multi-dimensional direct methods was also successful (Fan et al., 1993; Sha, et al., 1994).

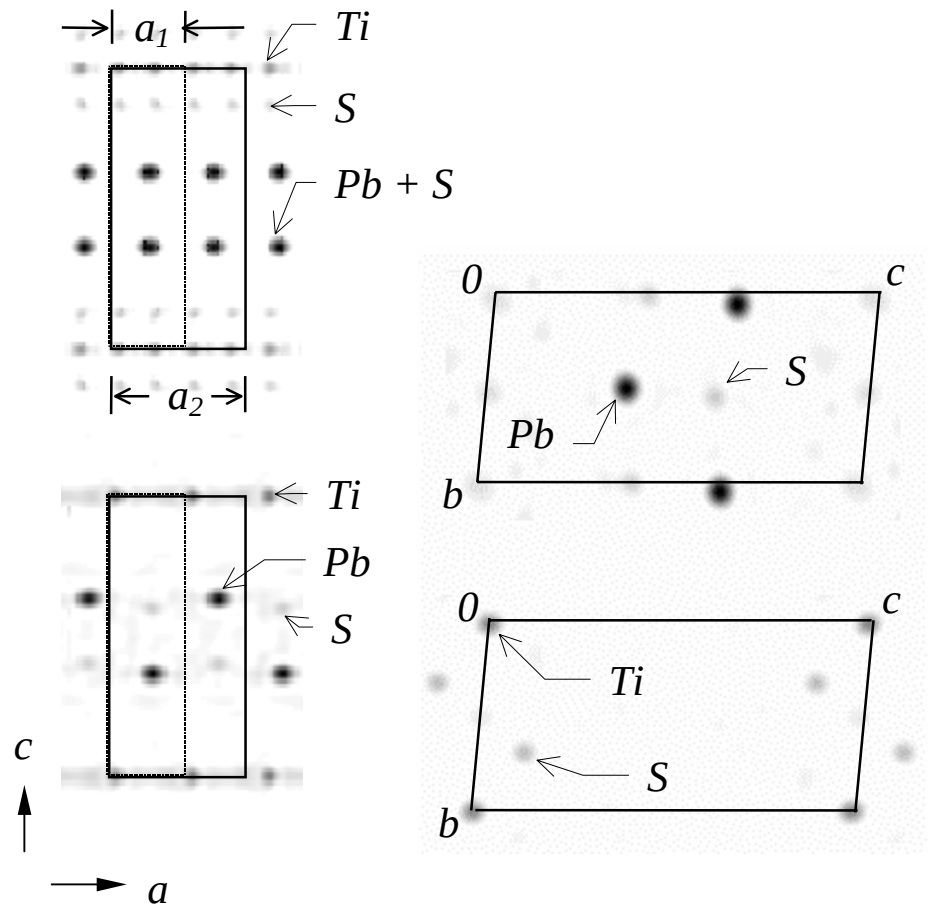

Figure 9. Direct-method phased Fourier maps of $(PbS)_{1.18}TiS_2$. Upper-left: $\int \rho(x_1,x_2,x_3,0)dx_2$, the 3-dimensional hypersection of the electron density function projected down the ***b*** axis; Lower-left: $\rho(x_1, 0, x_3\ 0)$; Upper-right: $\rho(0.25, x_2, x_3, 0.25)$; Lower-right: $\rho(0, x_2, x_3, 0)$.

ON THE EFFECT OF DYNAMICAL ELECTRON DIFFRACTION

It is well known that the dynamical diffraction effect causes serious problems in crystal-structure analysis using electron diffraction data. However, recent study (Li, Wan, Li and Fan, 1998) showed that this effect is often much weaker than what people would usually predict. The thermal motion of atoms, the incommensurate modulation of the structure and any deviation from the ideal periodicity can significantly weaken the dynamical diffraction effect. In practice many structural defects, which break the ideal periodicity, are either unrecognized or difficult to handle in simulating calculations. Hence the dynamical electron diffraction effect is often overestimated in theoretical considerations.

It is believed that, with kinematical electron-diffraction analysis, reasonable result is unlikely to be obtained from a sample much thicker than 100Å, especially when the sample contains heavy atoms. However, the following simulating calculation shows that, under the kinematical-diffraction approximation, the incommensurate modulation of Bi-2201 could be determined by using electron diffraction data from a sample as thick as 300Å. Details on the determination of the incommensurate modulation in Bi-2201 from experimental electron diffraction data have been given in the previous section. The resulting potential map is shown in Figure 8. Here we start from the resulting structure model. Atoms in which are expressed by their scattering factor, positional and thermal parameters, and their modulation parameters. Four different sets of dynamical diffraction intensities were calculated assuming respectively the sample thickness equal to 1×5.41Å (the length of the ***a*** axis), 20×5.41Å, 40×5.41Å and 60×5.41Å. Potential maps (shown in Figure 10) were then obtained by assigning the correct phases to the square roots of dynamical diffraction intensities. Figure 10*a*, which can be considered as nearly the true structure image, is close enough to the experimental map in Figure 8. The other three maps all have their essential feature similar to that of Figure 10*a*. Furthermore, even some oxygen atoms are visible on the map corresponding to the sample thickness of 300Å (Figure 10*d*). It turns out that, based on the kinematical-diffraction approximation, the modulation of all metal atoms in Bi-2201 could be determined by using electron diffraction data from a sample as thick as 300Å,

provided we can find the correct phases by whatever method. The complete structure may then be solved by Fourier recycling. Besides, given a rough structure model or just a partial structure, there are some techniques to compensate the dynamical diffraction effect (Sha, Fan and Li,1993; Huang, Liu, Gu, Xiong, Fan and Li, 1996). This would further improve the results.

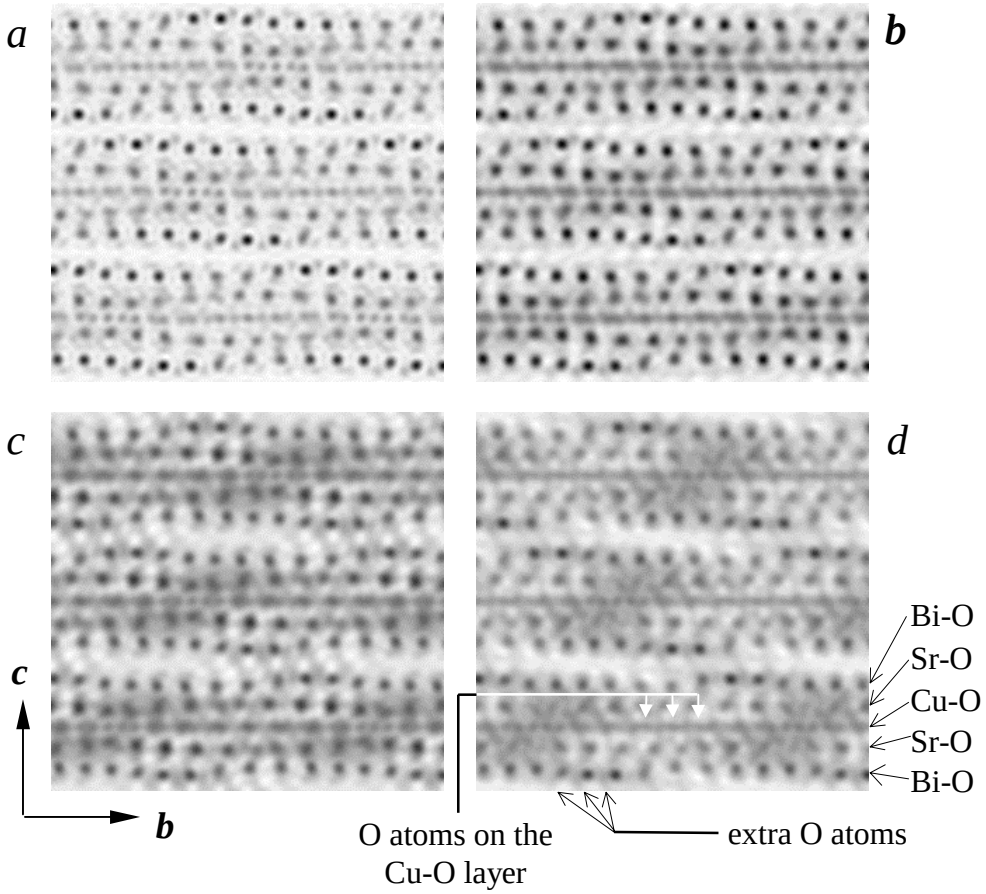

Figure 10. Simulating potential distribution of the superconductor Bi-2201 projected down the ***a*** axis on to an area of 7*b*×3*c*, calculated with the structure factors replaced by the square roots of dynamical diffraction intensities associated with correct phases. (a) sample thickness = 1×5.41Å; (b) sample thickness = 20×5.41Å; (c) sample thickness = 40×5.41Å; (d) sample thickness = 60×5.41Å.

The calculation, measurement and display of images shown in this paper, except for those in Figures 1, and 7, were done by the program *VEC* (Wan, Fu and Fan, 1997) running on an *IBM* compatible PC.

ACKNOWLEDGMENTS

The author should like to thank Z. H. Wan, Y. D. Liu and Y. Z. He, for their assistance in preparing the manuscript. The work was supported in part by the National Natural Science Foundation of China.

REFERENCES

Allpress, J. G., Hewat, E. A., Moodie, A. F and Sanders, J. V. (1972) *n*-Beam lattice images I. Experimental and computed images from $W_4Nb_{26}O_{77}$. Acta Cryst., *A28*: 528-536.

Cowley, J. M. (1953) Structure analysis of single crystals by electron diffraction. II. Disordered boric acid structure. Acta Cryst., *6*: 522-529.

Cowley, J. M. and Iijima S. (1972) Electron microscope image contrast for thin crystals. Z. Naturforsch., *A27*: 445-451.

De Wolff, P. M. (1974) The pseudo-symmetry of modulated crystal structures. Acta Cryst., *A30*: 777-785.

Dorset, D. L. and Hauptman H. A. (1976) Direct phase determination for quasi-kinematical electron diffraction intensity data from organic microcrystals. Ultramicroscopy, *1*: 195-201.

Dorset, D. L., Tivol, W. F. and Turner, J. N. (1991) Electron crystallography at atomic resolution: ab initio structure analysis of copper perchlorophthalocyanine. Ultramicroscopy, *38*: 41-45.

Dorset, D. L., Tivol, W. F. and Turner, J. N. (1992) Dynamical scattering and electron crystallography — ab initio structure analysis of copper perbromophthalocyanine. Acta Cryst., *A48*: 562-568.

Fan, H.F., and Li, F. H. (1987) Direct methods as a tool of image processing in high resolution microscopy. In: Schenk, H., Wilson A. J. C. and Pathasarathy, S. Eds. Direct Methods, Macromolecular Crystallography and Crystallographic Statistics, World Scientific, Singapore, pp. 400-409.

Fan, H. F., Van Smaalen, S., Lam, E. J. W. and Beurskens, P. T. (1993) Direct methods for incommensurate intergrowth compounds I. Determination of the modulation. Acta Cryst., *A49*: 704-708.

Fan, H. F. Xiang, S. B., Li, F. H., Pan, Q. Uyeda, N. and Fujiyoshi Y. (1991) Image resolution enhancement by combining information from electron diffraction pattern and micrograph. Ultramicroscopy, *36*: 361-365.

Fan, H. F. and Zheng, Q. T. (1975) Extrapolation of structure factors in diffraction analysis. Acta Phys. Sin., *24*: 97-104. (in Chinese)

Fan, H. F., Zhong, Z. Y., Zheng, C. D. and Li, F. H. (1985) Image processing in high resolution electron microscopy using the direct method I. Phase extension. Acta Cryst., *A41*: 163-165.

Fijes, P. L. (1977) Approximations for the calculation of high-resolution electron-microscopy images of thin films. Acta Cryst., *A33*: 109-113.

Fu, Z. Q. and Fan, H. F. (1994) *DIMS* — a direct method program for incommensurate modulated structures. J. Appl. Cryst., *27*: 124-127.

Fu, Z. Q. and Fan, H. F. (1997) A computer program to derive (3+1)-dimensional symmetry operations from two-line symbols. J. Appl. Cryst., *30*: 73-78.

Fu, Z. Q., Huang, D. X., Li, F. H., Li, J. Q., Zhao, Z. X., Cheng, T. Z. and Fan, H. F. (1994) Incommensurate modulation in minute crystals revealed by combining high resolution electron microscopy and electron diffraction. Ultramicroscopy, *54*: 229-236.

Fu, Z. Q., Li, Y., Cheng, T. Z., Zhang, Y. H., Gu, B. L. and Fan, H. F. (1995) Incommensurate modulation in Bi-2212 high Tc superconductor revealed by single crystal X-ray analysis using direct methods. Science in China, A38, 210-216.

Gao, Y., Coppens, P., Cox, D. E. and Moodenbaugh, A. R. (1993) Combined X-ray single-crystal and neutron powder refinement of modulated structures and application to the incommensurately modulated structure of $Bi_2Sr_2CaCu_2O_{8+y}$. Acta Cryst., *A49*: 141-148.

Gao, Y., Lee, P., Coppens, P., Subramanian, M. A. and Sleight, A. W. (1988) The incommensurate modulation of the 2212 Bi-Sr-Ca-Cu-O superconductor. Science, *241*: 954-956.

Gao, Y., Lee, P., Ye, J., Bush, P., Petricek, V. and Coppens, P. (1989) The incommensurate modulation in the $Bi_2Sr_{2-x}Ca_xCu_2O_6$ superconductor, and its relation to the modulation in $Bi_2Sr_{2-x}Ca_xCu_2O_8$. Physica C, *160*: 431-438.

Gassmann, J. (1976) Improvement and extension of approximate phase sets in structure determination. In: Ahmed, F. R., Ed. Crystallographic Computing Techniques, Munksgaard, Copenhagen, pp. 144-154.

Gerchburg, R. W. and Saxton W. O. (1971) Phase determination from image and diffraction plane pictures in the electron microscope. Optik, *34*: 275-284.

Han, F. S., Fan H. F. and Li, F. H. (1986) Image processing in high resolution electron microscopy using the direct method II. Image deconvolution. Acta Cryst., *A42*: 353-356;

Hao, Q., Liu, Y. W. and Fan, H. F. (1987) Direct methods in superspace I. Preliminary theory and test on the determination of incommensurate modulated structures. Acta Cryst., *A43*: 820-824;

Huang, D. X., Liu, W., Gu, Y. X., Xiong, J. W., Fan, H. F. and Li, F. H. (1996) A method of electron diffraction intensity correction in combination with high resolution electron microscopy. Acta Cryst., *A52*: 152 - 157

Ishizuka K., Miyazaki, M. and Uyeda, N. (1982) Improvement of electron microscope image by the direct phasing method. Acta Cryst., *A38*: 408-413.

Janssen, T., Janner, A., Looijenga-Vos, A. and De Wolff, P. M. (1992) Incommensurate and commensurate modulated structures. In: Wilson, A. J. C. Ed. International Tables for Crystallography, Vol. C, Kluwer Academic Publishers, Dordrecht, pp. 797-835; 843-844.

Kan, X. B. and Moss, S. C. (1992) Four-dimensional crystallographic analysis of the incommensurate modulation in a $Bi_2Sr_2CaCu_2O_8$ single crystal. Acta Cryst., *B48*: 122-134.

Karle, J. and Hauptman, H. (1956) A theory of phase determination for the four types of non-centrosymmetric space groups 1P222, 2P22, $3P_12$, $3P_22$. Acta Cryst., *9*: 635-651.

Li, F. H. and Fan, H. F. (1979) Image deconvolution in high resolution electron microscopy by making use of Sayre's equation. Acta Phys. Sin., *28*: 276-278. (in Chinese)

Li, J. Q., Yang, D. Y., Li, F. H., Zhou, P., Zheng, D. N., Ni, Y. M., Jia, S. L. and Zhao, Z. X. (1989) Structure Symmetry and microstructures of Bi(Pb)-Sr-Ca-Cu-O system. Progress in High Tc Superconductivity, *22*: 441-443.

Li, Y., Wan, Z. H., Li, F. H. and Fan, H. F. (1999) On the effect of dynamical electron diffraction. (to be submitted).

Liu, Y. W., Xiang, S. B., Fan, H. F., Tang, D., Li, F. H. Pan, Q., Uyeda, N. and Fujiyoshi, Y. (1990) Image deconvolution of a single high resolution electron micrograph. Acta Cryst., *A46*: 459-463.

Liu, Y. W., Fan, H. F. and Zheng, C. D. (1988) Image processing in high resolution electron microscopy using the direct method III. Structure factor extrapolation. Acta Cryst., *A44*: 61-63.

Matsui, Y. and Horiuchi, S. (1988) Geometrical relations of various modulated structures in Bi-Sr-Ca-Cu-O Superconductors and related compounds. Jpn. J. Appl. Phys., ***27***: L2306-L2309.

Mo, Y. D., Cheng, T. Z., Fan, H. F., Li, J. Q., Sha, B.D., Zheng, C. D., Li, F. H. and Zhao, Z. X. (1992) Structural features of the incommensurate modulation in Pb-doped Bi-2223 high-Tc phase revealed by direct-method electron diffraction analysis. Supercond. Sci. Technol., *5*: 69-72.

Mo, Y. D., Fu, Z. Q., Fan, H. F., Van Smaalen, S., Lam, E. J. W. and Beurskens, P. T. (1996) Direct methods for incommensurate intergrowth compounds III. Solving the average structure in multidimensional space. Acta Cryst., *A52*: 640-644.

Petricek, V., Gao, Y., Lee, P. and Coppens, P. (1990) X-ray analysis of the incommensurate modulation in the 2:2:1:2 Bi-Sr-Ca-Cu-O superconductor including the oxygen atoms. Phys. Rev., *B42*: 387-392.

Sayre, D. (1952) The squaring method: a new method for phase determination. Acta Cryst., *5*: 60-65.

Sequeira, A., Yakhmi, J. V., Iyer, R. M., Rajagopal, H. and Sastry, P. V. P. S. S. (1990) Novel structural features of Pb-stabilised Bi-2223 high-*T*c phase from neutron-diffraction study. Physica Scripta, *C167*: 291-296.

Sha, B. D., Fan, H. F., Van Smaalen, S., Lam, E. J. W. and Beurskens, P. T. (1994) Direct methods for incommensurate intergrowth compounds II. Determination of the modulation using only main reflections. Acta Cryst., *A50*: 511-515.

Sha, B. D., Fan, H. F. and Li, F. H. (1993) Correction of dynamical electron diffraction effect in crystal structure analysis. Acta Cryst., *A49*: 877-880.

Tivol, W. F., Dorset, D. L., McCourt, M. P. and Turner, J. N. (1993) Voltage-dependent effects on dynamical scattering and the electron diffraction structure analysis of organic crystals: Copper perchlorophthalocyanine. MSA Bulletin *23*: 91-98.

Uyeda, N. and Ishizuka, K. (1974) Correct molecular image seeking in the arbitrary defocus series. In: Sanders, J. V. and Goodchild, D. J. Eds. Eighth Int. Congr. Electron Microscopy, Vol.1, pp. 322-323.

Uyeda, N. and Ishizuka, K. (1975) Molecular image reconstruction in high resolution electron microscopy. J. Electron Microscopy, *24*: 65-72.

Uyeda N., Kobayashi, T., Suito E., Harada, Y. and Watanabe, M. (1972) Molecular resolution in electron microscopy. J. Appl. Phys., *43*: 5181-5189.

Vainshtein, B. K. (1964) Structure Analysis by Electron Diffraction, Pergamon, Oxford.

Van Smaalen, S. (1992) Superspace description of incommensurate intergrowth compounds and the application to inorganic misfit layer compounds. Mater. Sci. Forum, *100–101*: 173-222.

Van Smaalen, S., Meetsma, A., Wiegers, G. A. and De Boer, J. L. (1991) Determination of the modulated structure of the inorganic misfit layer compound $(PbS)_{1.18}TiS_2$. Acta Cryst., *B47*: 314-325.

Wan, Z. H., Fu, Z. Q. and Fan, H. F. (1997) *VEC*. A program for visual computing in electron crystallography. Institute of Physics, Beijing, China.

Woolfson, M. M. and Fan, H. F. (1995) Physical and Non-Physical Methods of Solving Crystal Structures, Cambridge Univ. Press, Cambridge, pp.106-107.

Yamamoto, A. (1982) Structure factor of modulated crystal structures. Acta Cryst., *A38*: 87-92.

Yamamoto, A., Onoda, M., Takayama-Muromachi, E., Izumi, F., Ishigaki, T. and Asano, H. (1990) Rietveld analysis of the modulated structure in the superconducting oxide $Bi_2(Sr,Ca)_3Cu_2O_{8+x}$. Phys. Rev., *B42*: 4228-4239.

Yamamoto, A., Takayama-Muromachi, E., Izumi, F., Ishigaki, T. and Asano, H. (1992) Rietveld analysis of the composite crystal in superconducting $Bi_{2+x}Sr_{2-x}CuO_{6+y}$. Physica C, *201*: 137-144.

Yao, J. X. (1981) On the application of phase relationships to complex structures XVIII. *RANTAN—Random MULTAN*. Acta Cryst., *A37*: 642-644.